Fırat Üniversitesi Deneysel ve Hesaplamalı Mühendislik Dergisi

FUJECE

# Karma Mimarideki Çok-Girişli Çok-Çıkışlı Sistemde Seyrek Sinyal Geriçatım Yöntemlerini Kullanarak Milimetrik Dalga Kanalı Uzamsal Kovaryansının Kestirilmesi

Rıfat Volkan ŞENYUVA[1]*

[1]Elektrik-Elektronik Mühendisliği Bölümü, Mühendislik ve Doğa Bilimleri Fakültesi, Maltepe Üniversitesi, İstanbul, Türkiye.
[1]rifatvolkansenyuva@maltepe.edu.tr

Geliş Tarihi: 21.01.2024
Kabul Tarihi: 7.06.2024

Düzeltme Tarihi: 29.03.2024

doi: https://doi.org/10.62520/fujece.1423312
Araştırma Makalesi

Alıntı: R. V. Şenyuva, "Karma mimarideki çok-girişli çok-çıkışlı sistemde seyrek sinyal geriçatım yöntemlerini kullanarak milimetrik dalga kanalı uzamsal kovaryansının kestirilmesi", Fırat Üni. Deny. ve Hes. Müh. Derg., vol. 4, no 1, pp. 30-43, Şubat 2025.

**Öz**

Bu çalışmada milimetrik dalga bandını kullanan darbant haberleşme sisteminde tek bir kullanıcıya ait kanalın kovaryans kestirimi incelenmektedir. Haberleşme sistemi zaman bölüşümlü çalışmaktadır ve kullanıcıdan baz istasyonu yönündeki kanal için kovaryans kestirimi yapılmaktadır. Baz istasyonu çok antenli ve radyo frekans (RF) zinciri hem analog hem sayısal birleştiricilerden oluşan çok-girişli çok-çıkışlı karma mimariye sahipken, kullanıcının tek anteni vardır. Ele alınan sistem modelinde ortak birleştirici matris yönteminin, milimetrik dalga kanalı uyum süresi boyunca gönderilen pilot bloklar için aynı birleştirici matrisinin uygulanması, kullanıldığı varsayılmaktadır. Seyrek sinyal geriçatım yöntemlerinden eşzamanlı normal uyum kovalama, çok ölçümlü seyrek Bayes öğrenme ve korelasyonlu seyrek Bayes öğrenmenin sistem modeline uygulanışı gösterilmektedir. İncelenen yöntemlerin sayısal sonuçları hesaplanarak normalleştirilmiş en küçük ortalama karesel hata başarımları değişen RF zincir sayısı ve milimetrik kanal seyreklik oranları için referans en küçük ortalama kare (EKOK) kestiricisiyle karşılaştırılmaktadır. Sayısal sonuçlar tüm deneylerde referans EKOK kestiricisine en yakın başarımların, korelasyonlu seyrek Bayes öğrenmeye ait olduğunu göstermektedir.

**Anahtar kelimeler:** Milimetrik dalga, Uzamsal kanal kovaryansı, Seyrek sinyal geriçatımı, Karma önkodlama

*Yazışılan Yazar

İntihal Kontrol: Evet – Turnitin
Şikayet: fujece@firat.edu.tr

*Firat Univ Jour. of Exp. and Comp. Eng., 4(1), 30-43, 2025*

Firat University Journal of Experimental and Computational Engineering

# Covariance Estimation Of Millimeter Wave Channels Using Sparse Signal Recovery Algorithms In A Hybrid MIMO Architecture

Rıfat Volkan ŞENYUVA [1*]

[1]Department of Electrical-Electronics Engineering, Faculty of Engineering and Natural Sciences, Maltepe University, Istanbul, Türkiye.
[1]rifatvolkansenyuva@maltepe.edu.tr

Received: 21.01.2024
Accepted: 7.06.2024
Revision: 29.03.2024
doi: https://doi.org/10.62520/fujece.1423312
Research Article

Citation: R. V. Senyuva, "Covariance estimation of millimeter wave channels using sparse signal recovery algorithms in a hybrid MIMO architecture", Firat Univ. Jour. of Exper. and Comp. Eng., vol. 4, no 1, pp. 30-43, February 2025.

## Abstract

In this paper, the channel covariance estimation of a single mobile station (MS) in a narrowband millimeter wave (mmWave) communication system was addressed. The communication system worked in time division duplex (TDD) mode and the channel covariance was estimated in the uplink communication. The base station (BS) had multiple antennas with a hybrid architecture of radio frequency (RF) chains made up of analog and digital combiners, while the MS had a single antenna. The investigated system model assumed the shared combining matrix scheme where the same combining matrix was used across multiple coherence blocks of the mmWave channel. The application of the sparse signal recovery algorithms including the simultaneous orthogonal matching pursuit (SOMP), the multiple response sparse Bayesian learning (MSBL), and the correlated sparse Bayesian learning (CSBL) to the system model were shown. The algorithms were evaluated numerically, and their normalized mean square error (NMSE) performances were compared against the benchmark oracle minimum mean square error (MMSE) estimator in multiple scenarios of varying number of RF chains at the BS and sparsity ratios for modeling the mmWave channel. The numerical results indicated that the CSBL algorithm provided the NMSE results closest to that of the oracle MMSE estimator in all the scenarios.

**Keywords:** Millimeter wave, Spatial channel covariance, Sparse signal recovery, Hybrid precoding

*Corresponding author

## 1. Introduction

Millimeter wave (mmWave) communication is one of the technologies considered for next-generation wireless systems [1-2]. The high data rate requirements of the next-generation wireless systems can be satisfied with the mmWave communication where the frequencies from 30 GHz up to 300 GHz with bandwidths as large as 2 GHz can be assigned to systems [1-2]. The signal processing at the mmWave frequencies is much more challenging than at lower frequencies due to new hardware constraints, different channel models, and the usage of large arrays. The power consumption and the high costs of circuits are important hardware constraints and to deal with them, the signal processing operations can be separated into analog and digital domains so that the number of analog-to-digital converters (ADC) can be reduced, or low-resolution ADCs may be used [3-5]. These hardware constraints have renewed the interest in the research of hybrid beamforming [6-7] and low-rate ADC methods [3-5]. The mmWave channel models must consider the drastic path loss due to attenuation at these frequencies. This makes estimation of the channel state information (CSI) of the mmWave systems very difficult since the signal-to-noise ratio (SNR) is poor without any application of beamforming. To mitigate the high propagation losses and improve the SNR, the mmWave systems need high beamforming gains which can only be achieved via large antenna arrays. These systems must employ hybrid analog-digital precoding techniques [6-7] to decrease the number of radio frequency (RF) chains needed at each antenna of the array so that the hardware costs can be maintained. The accurate full CSI is critical for the performance of these hybrid precoding techniques. Since the number of RF chains is less than the number of antennas in these hybrid systems, the received signal is lower dimensional which makes obtaining the full CSI even more challenging. There exist other hybrid precoding techniques which use spatial channel covariance instead of the full CSI. Thus, the channel covariance estimation is crucial in reaping the benefits of the hybrid mmWave systems.

A mmWave channel can be modeled as a sparse signal in the angular domain since the signals arrive in a small number of path clusters due to limited scatterers around the receiver. There is also spatial correlation since the antennas in the array are close to each other. Each signal with an angle of arrival correspond to a spatial frequency and the continuous domain of the spatial frequencies can be discretized into a finite set of grid points. If the true spatial frequencies are close to some of the grid points, the received signal at the $t$-th snapshot, $\tilde{\mathbf{y}}_t \in \mathbb{C}^{M\times 1}$, can be given as a linear system of equation,

$$\tilde{\mathbf{y}}_t = \mathbf{\Phi}_t \mathbf{g}_t + \mathbf{z}_t, \qquad t = 1, \dots, T. \tag{1}$$

In Equation (1), $\mathbf{\Phi}_t \in \mathbb{C}^{M\times D}$ is the known dictionary matrix, $\mathbf{g}_t \in \mathbb{C}^{D\times 1}$ is the unknown mmWave channel vector, and the noise is shown as $\mathbf{z}_t \in \mathbb{C}^{M\times 1}$. This system of equations is underdetermined due to the reducing the number of RF chains via the hybrid precoding, i.e. $M \leq D$, and the unknown parameter vector $\mathbf{g}_t$ is sparse with only $L \ll D$ nonzero entries. The covariance matrix, that determines the spatial correlation between the components of the channel vector, is assumed to remain constant during $t = 1, \dots, T$ snapshots. Finding a single solution amongst infinitely many requires imposing additional constraints in these underdetermined systems. Since the unknown mmWave channel vector is sparse, its nonzero entries can be estimated by applying the sparse signal recovery algorithms to Equation (1).

The point estimates of the correlated sparse mmWave channel of a single user can be obtained via the orthogonal matching pursuit (OMP) based algorithm proposed in [8]. However, the selection of the dictionary matrix, which must be done according to the restricted isometry property, determines the accuracy of the solutions provided by the OMP based algorithms. [9] proposes covariance estimation methods based on the simultaneous OMP (SOMP) algorithm for both fixed and varying dictionary matrices at each snapshot. The grid mismatch issue associated with the generation of the dictionary matrix for the greedy OMP and SOMP algorithms are addressed in the works [10-12]. While [10] proposes grid-less refinement steps for the OMP algorithm and a perturbation framework is given by [11] for the SOMP algorithm, [12] shows the implementation of a multigrid dictionary refinement scheme to be used with the SOMP algorithm. The out-of-band covariance information translated from a parallel sub-6 GHz system is used in the sparse recovery of the covariance of the wideband mmWave multiple-input multiple-output (MIMO) channel [13]. Multiple sparse Bayesian learning (MSBL) framework [14] utilizes expectation-maximization (EM) to find

probabilistic estimates of the unknown channel vector in Equation (1). Although the MSBL algorithm is more resilient to the selection of the dictionary matrix compared to the OMP based solutions, it uses a diagonal prior covariance matrix and so does not take the spatial correlation of the channel vector into account. The temporal correlation between the entries of the unknown channel vectors at different snapshots is considered in [15] where the measurement matrix made up from $T$ measurements in Equation (1) is vectorized and a block MSBL algorithm is proposed. The correlated SBL (CSBL) algorithm [16] improves upon the MSBL algorithm by using a prior covariance matrix which is not diagonal and a much better model for the spatial correlation between the entries of the unknown channel vector. The CSBL algorithm has a computational disadvantage over the MSBL algorithm that it requires explicit calculation of the inverse of a precision matrix. A faster version of the CSBL algorithm with reduced complexity is proposed in [17]. The impact of the residual transceiver impairments in the components of the RF chain is examined for a narrowband mmWave hybrid MIMO system in [18]. A zero-attracting least mean square (ZALMS) adaptive filtering algorithm is proposed for the estimation of the downlink channel [18].

The covariance estimation of the mmWave channels in a narrowband hybrid MIMO communication system is investigated in this paper. In our system model a single mobile station (MS) with a single antenna is communicating to a base station (BS) with a mixture of analog and digital combiners in its RF chains and the estimation takes place during the uplink communication. Since the communication system works in time-division duplex (TDD) mode, the channel reciprocity allows the downlink communication to be precoded with the estimated uplink channel. The combining matrix is assumed to be shared across multiple pilot blocks transmitted by the MS within the coherence of the mmWave channel. We focus on covariance estimation methods using sparse signal reconstruction and show how the SOMP, the MSBL, and the CSBL algorithms can be applied to estimate the mmWave channel of a single MS communicating to a hybrid MIMO BS using the shared combining matrix scheme. The performances of the algorithms are compared in multiple scenarios with varying number of RF chains and mmWave channels with varying sparsity levels.

The remainder of this paper is arranged as: the models of the hybrid MIMO system and the mmWave channel are explained in Section 2. Then, the mmWave channel covariance estimation methods based on sparse signal recovery are presented in Section 3. The numerical evaluations of the methods are given in Section 4. Finally, Section 5 is the conclusions.

## 2. System Model

We consider a narrowband communication system operating in half-duplex TDD mode where either the BS or the MS is transmitting at one time. The total number of samples available within the coherence interval of the channel are divided into three subintervals: uplink data, uplink pilot, and downlink data [19]. The BS learns the CSI of the uplink channel via the symbols transmitted by the MS in the uplink pilot's subinterval of the coherence interval. Once the BS has the acquired the uplink channel, it also has an estimate of the downlink channel due to the channel reciprocity that is the impulse response of the channel between any two antennas is the same [19]. In both uplink and downlink data transmissions, all complexity resides in the BS. In the uplink data transmission, the MS sets its power level and then transmits the data symbols, and the BS decodes the received symbols via either zero-forcing or maximum-ratio combining using the uplink channel estimate. Similarly in the downlink data transmission, the BS applies a linear precoding operation using either zero-forcing or maximum-ratio combining on the information bearing symbols before transmission [19]. The BS has a uniform linear array (ULA) of $N$ antennas placed at equal distance from each other and $M$ hybrid RF chains. An RF chain consists of components such as low-noise amplifiers, filters, mixers, converters, oscillators, ADCs, and automatic gain control [1,13,18]. The analog combiner connecting the antennas of the BS to its RF chains in Figure 1 is the RF combiner and it can be implemented using phase shifters which imposes unit norm entries in the analog combining matrix [1,18]. To convert the output of the RF chains to baseband, the BS must apply a second baseband combiner before the covariance of the channel can be estimated. The BS is communicating with a single MS which has a single antenna (Figure 1).

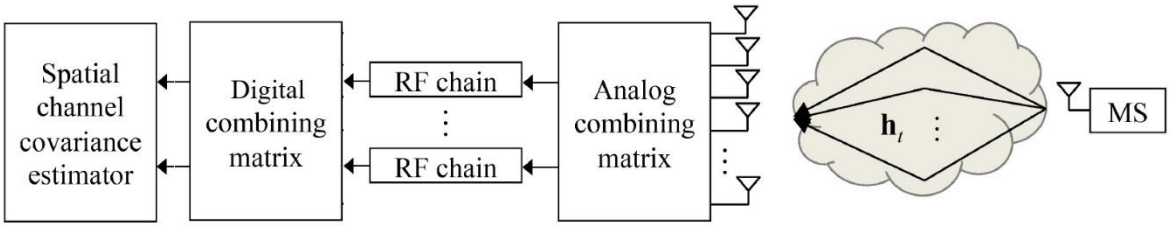


**Figure 1.** BS has $N$ antennas and $M$ RF chains while there is only a single antenna at the MS. The mmWave channel is represented with a narrowband geometric channel with $L$ paths and the estimation of the channel covariance occurs in baseband [9]

The uplink mmWave channel from the MS and the BS is modeled according to the geometric channel model with $L$ number of channel paths (Figure 1) as

$$\mathbf{h}_t = \sum_{l=1}^{L} \bar{g}_{t,l}\mathbf{b}(\phi_l) = \mathbf{B}\bar{\mathbf{g}}_t \tag{2}$$

where $\bar{\mathbf{g}}_t = [\bar{g}_{t,1} \quad \cdots \quad \bar{g}_{t,L}]^{\mathrm{T}} \in \mathbb{C}^{L\times 1}$, $\bar{g}_{t,l}$ shows the gain of the $l$-th channel path at the $t$-th snapshot, and $\mathbf{B} = [\mathbf{b}(\phi_1) \quad \cdots \quad \mathbf{b}(\phi_L)] \in \mathbb{C}^{N\times L}$. A column of $\mathbf{B}$, i.e. $\mathbf{b}(\phi_l)$, is the array steering vector associated with the angle-of-arrival (AoA) of the $l$-th channel path, i.e. $\phi_l$, is

$$\mathbf{b}(\phi_l) = [1 \quad e^{-i\pi\cos\phi_l} \quad \ldots \quad e^{-i\pi(N-1)\cos\phi_l}]^{\mathrm{T}} \tag{3}$$

In Equation (3) the spacing between the elements of the ULA at the BS is assumed to be equal to half of the wavelength and it is also assumed that the AoAs do not change for $T$ snapshots.

A dictionary matrix, $\mathbf{A} = [\mathbf{a}(\phi_1) \quad \cdots \quad \mathbf{a}(\phi_D)] \in \mathbb{C}^{N\times D}$ can be built by creating a grid of $D \gg L$ points on the range of the spatial frequencies, i.e. $\mu_l = \cos\phi_l$, from -1 to +1 and Equation (2) can be rewritten using this dictionary matrix as

$$\mathbf{h}_t = \mathbf{A}\mathbf{g}_t \tag{4}$$

The path gain vector, $\mathbf{g}_t \in \mathbb{C}^{D\times 1}$, in Equation (4) has a support, the set of indices indicating to the nonzero entries, $\mathcal{S} = \left\{j: g_{t_j} \neq 0\right\}$, with $L$ elements $|\mathcal{S}| = L$ and they correspond to the AoAs, $\{\phi_1, \ldots, \phi_D\}$. The covariance matrix of the channel, $\mathbf{R}_\mathbf{h} \in \mathbb{C}^{N\times N}$, can be written as

$$\mathbf{R}_\mathbf{h} = \mathbb{E}\{\mathbf{h}_t\mathbf{h}_t^*\} = \mathbf{A}\mathbf{R}_\mathbf{g}\mathbf{A}^* \tag{5}$$

in terms of $\mathbf{R}_\mathbf{g} = \mathbb{E}\{\mathbf{g}_t\mathbf{g}_t^*\} \in \mathbb{C}^{D\times D}$, the covariance matrix of the path gains. $(\cdot)^*$ shows the Hermitian transpose. We assume that the components of the path gain vector, $\mathbf{g}_t$, are correlated with each other and so the entries of the covariance matrix are given as $\left[\mathbf{R}_\mathbf{g}\right]_{(j,k)} = \rho_{j,k}\sqrt{\gamma_j}\sqrt{\gamma_k}$ where $\rho_{j,k}$ is correlation coefficient between the entries and $\gamma_j$ is the variance of the $j$-th entry. The covariance matrix of the path gains can be written in matrix form as

$$\mathbf{R}_\mathbf{g} = \mathbf{\Gamma}^{1/2}\mathbf{U}\mathbf{\Gamma}^{1/2} \tag{6}$$

where $\mathbf{\Gamma}^{1/2} = \mathrm{diag}\{\sqrt{\gamma_1}, \ldots, \sqrt{\gamma_D}\}$ and the entries of $\mathbf{U}$ are $[\mathbf{U}]_{(j,k)} = \rho_{j,k}$.

The MS transmits a unit modulus pilot symbol, i.e. $|x_t| = 1$, and the received signal at the BS is

$$\mathbf{y}_t = \mathbf{A}\mathbf{g}_t x_t + \mathbf{n}_t \tag{7}$$

where $\mathbf{n}_t \in \mathbb{C}^{N\times 1}$ is the additive complex circularly symmetric Gaussian noise vector with the single-sided spectral density of each of its component being $N_0$, i.e. $\mathbf{n}_t \sim \mathcal{CN}(\mathbf{0}, N_0\mathbf{I})$. The received signal is multiplied with a hybrid combining matrix, $\mathbf{W}_t = \mathbf{W_{BB}}\mathbf{W_{RF}} \in \mathbb{C}^{M\times N}$, which is a cascade of the analog, $\mathbf{W_{RF}} \in \mathbb{C}^{M\times N}$, and digital, $\mathbf{W_{BB}} \in \mathbb{C}^{M\times M}$, combining matrices (Figure 1) and the conjugate of the pilot symbol, $x_t^*$, so that the result of this operation is the signal at baseband given as

$$\tilde{\mathbf{y}}_t = \mathbf{W}_t\mathbf{A}\mathbf{g}_t x_t x_t^* + \mathbf{W}_t\mathbf{n}_t x_t^* = \mathbf{\Phi}_t\mathbf{g}_t + \mathbf{z}_t \tag{8}$$

where the overall sensing matrix is shown as $\mathbf{\Phi}_t = \mathbf{W}_t\mathbf{A} \in \mathbb{C}^{M\times D}$ and the new noise vector, $\mathbf{z}_t = x_t^*\mathbf{W}_t\mathbf{n}_t \in \mathbb{C}^{M\times 1}$, is distributed as $\mathbf{z}_t \sim \mathcal{CN}(\mathbf{0}, |x_t|^2 N_0 \mathbf{W}_t\mathbf{W}_t^*)$. The conjugate transpose of a matrix is shown by superscript $(\cdot)^*$. Assuming that there are $T$ snapshots in total and the hybrid combining matrix is fixed for each snapshot that is $\mathbf{W}_1 = \cdots = \mathbf{W}_T = \mathbf{W}$, then the received signal vectors for $t = 1, \ldots, T$ in Equation (8) can be rewritten as

$$\tilde{\mathbf{Y}} = \mathbf{\Phi}\mathbf{G} + \mathbf{Z} \tag{9}$$

where the measurements are shown as $\tilde{\mathbf{Y}} = [\tilde{\mathbf{y}}_1 \ldots \tilde{\mathbf{y}}_T] \in \mathbb{C}^{M\times T}$, the dictionary matrix is $\mathbf{\Phi} = \mathbf{W}\mathbf{A} \in \mathbb{C}^{M\times D}$, $\mathbf{G} = [\mathbf{g}_1 \ldots \mathbf{g}_T] \in \mathbb{C}^{D\times T}$, and $\mathbf{Z} = [\mathbf{z}_1 \ldots \mathbf{z}_T] \in \mathbb{C}^{M\times T}$. The channel covariance estimation problem is to estimate $\mathbf{R_h}$ given $\tilde{\mathbf{Y}}$.

## 3. Covariance Estimation Using Sparse Signal Reconstruction

Equation (9) is a multiple measurement vector problem, and the optimum solution can be found from

$$\min_{\tilde{\mathbf{G}}} \left\|\tilde{\mathbf{Y}} - \mathbf{\Phi}\tilde{\mathbf{G}}\right\|_F \quad \text{subject to } \left\|\tilde{\mathbf{G}}\right\|_{\text{row}-0} \le L \tag{10}$$

where the Frobenius norm of a matrix, $\tilde{\mathbf{Y}}$, is shown as $\left\|\tilde{\mathbf{Y}}\right\|_F = \left(\sum_m^M \sum_t^T \left|\tilde{y}_{m,t}\right|^2\right)^{1/2}$ and the row-$\ell_0$ quasi-norm of a matrix is defined as $\left\|\tilde{\mathbf{G}}\right\|_{\text{row}-0} = \left|\text{rowsupp}(\tilde{\mathbf{G}})\right|$ [7,16]. The row support of a matrix, $\tilde{\mathbf{G}}$, is the set of indices for its nonzero rows that is

$$\text{rowsupp}(\tilde{\mathbf{G}}) = \left\{j : [\tilde{\mathbf{G}}]_{(j,k)} \neq 0 \text{ for some } k\right\} \tag{11}$$

### 3.1. SOMP algorithm

The SOMP algorithm shown solves Equation (10). In each iteration the SOMP algorithm first finds the column of the dictionary matrix, $\mathbf{\Phi}$, that is best aligned with the current residual matrix $\mathbf{V}$ [9,20-21] that is

$$j = \underset{d}{\text{argmax}} \|\phi_d^*\mathbf{V}\|_2, \quad d = 1, \ldots, D. \tag{12}$$

The index set, $\Lambda$, is updated with the index of the best aligned column from Equation (12). Then a new residual is calculated by removing the projection of the measurement matrix along the direction of the chosen columns

$$\mathbf{V} = (\mathbf{I} - \mathbf{\Phi}_\Lambda\mathbf{\Phi}_\Lambda^*)\tilde{\mathbf{Y}} \tag{13}$$

where $\mathbf{\Phi}_\Lambda$ is the submatrix constructed from the columns of $\mathbf{\Phi}$ that correspond to the indices in the set, $\Lambda$ [9,20-21].

The steps of the SOMP algorithm are shown in Figure 2. The SOMP algorithm iterates between steps 5-7. The computational complexity is dominated by the orthogonalization during the update of the residual matrix

in step 7. To reduce the computational complexity, the matrix decompositions such as Cholesky or QR can be applied. The SOMP algorithm implementing the QR matrix decomposition can terminate with a solution in $O(DML)$ operations [21].

1. **begin**
2. **input:** $\mathbf{\Phi} = \mathbf{WA}$, $\widetilde{\mathbf{Y}}$, $L$
3. **initialize:** $\mathbf{V} = \widetilde{\mathbf{Y}}$, $\Lambda = \emptyset$, $\widehat{\mathbf{G}}_{\mathrm{SOMP}} = \mathbf{0}$
4. **for** $l = 1{:}\,L$ do
5. $\quad j = \underset{d}{\operatorname{argmax}} \|\phi_d^* \mathbf{V}\|_2$
6. $\quad \Lambda = \Lambda \cup \{j\}$
7. $\quad \mathbf{V} = (\mathbf{I} - \mathbf{\Phi}_\Lambda \mathbf{\Phi}_\Lambda^*)\widetilde{\mathbf{Y}}$
8. **end for**
9. $\left[\widehat{\mathbf{G}}_{\mathrm{SOMP}}\right]_{(\Lambda,:)} = \mathbf{\Phi}_\Lambda^* \widetilde{\mathbf{Y}}$
10. **output:** $\widehat{\mathbf{G}}_{\mathrm{SOMP}}$, $\widehat{\mathbf{H}}_{\mathrm{SOMP}} = \mathbf{A}_\Lambda \widehat{\mathbf{G}}_{\mathrm{SOMP}}$

**Figure 2.** The pseudocode of the SOMP algorithm

Once the path gains, $\mathbf{g}_t$' s are estimated via $\widehat{\mathbf{G}}_{\mathrm{SOMP}}$, then the covariance channel matrix can be found using $\widehat{\mathbf{R}}_{\mathbf{g}} = (1/T)\widehat{\mathbf{G}}_{\mathrm{SOMP}}\widehat{\mathbf{G}}_{\mathrm{SOMP}}^*$ as in

$$\widehat{\mathbf{R}}_{\mathbf{h}} = \mathbf{A}\widehat{\mathbf{R}}_{\mathbf{g}}\mathbf{A}^* \tag{14}$$

## 3.2. MSBL algorithm

The MSBL algorithm calculates the maximum a posteriori (MAP) estimates of the channel path gains using the expectation-maximization (EM) method [14-15]. Given $\tilde{\mathbf{y}}_t$, the posterior conditional density of the path gain vector, $\mathbf{g}_t$, is circularly symmetric complex Gaussian with $\mathbf{g}_t \sim \mathcal{CN}(\boldsymbol{\mu}_{\mathrm{MSBL}_t}, \mathbf{\Sigma}_{\mathrm{MSBL}})$ [14]. The expectation step (E-step) of the MSBL algorithm calculates the mean and the covariance of the Gaussian distribution according to

$$\boldsymbol{\mu}_{\mathrm{MSBL}_t} = \mathbf{\Gamma}_{\mathrm{MSBL}} \mathbf{\Phi}^* \mathbf{\Omega}_{\mathrm{MSBL}}^{-1} \tilde{\mathbf{y}}_t \tag{15}$$

$$\mathbf{\Sigma}_{\mathrm{MSBL}} = \mathbf{\Gamma}_{\mathrm{MSBL}} - \mathbf{\Gamma}_{\mathrm{MSBL}} \mathbf{\Phi}^* \mathbf{\Omega}_{\mathrm{MSBL}}^{-1} \mathbf{\Phi} \mathbf{\Gamma}_{\mathrm{MSBL}} \tag{16}$$

respectively. In Equations (15) and (16), $\mathbf{\Gamma}_{\mathrm{MSBL}} = \mathrm{diag}\{\hat{\boldsymbol{\gamma}}_{\mathrm{MSBL}}\} \in \mathbb{C}^{D \times D}$ and $\mathbf{\Omega}_{\mathrm{MSBL}} = N_0 \mathbf{I} + \mathbf{\Phi} \mathbf{\Gamma}_{\mathrm{MSBL}} \mathbf{\Phi}^* \in \mathbb{C}^{M \times M}$ [14]. The maximization step (M-step) of the algorithm updates $\hat{\boldsymbol{\gamma}}_{\mathrm{MSBL}} = [\hat{\gamma}_1, \dots, \hat{\gamma}_D]$ according to

$$\hat{\gamma}_d = \frac{1}{T} \left\| [\mathbf{M}_{\mathrm{MSBL}}]_{(d,:)} \right\|_2^2 + [\mathbf{\Sigma}_{\mathrm{MSBL}}]_{(d,d)}, d = 1, \dots D \tag{17}$$

The posterior mean matrix shown as $\mathbf{M}_{\mathrm{MSBL}}$ in Equation (17) is the concatenation of the mean vectors that is $\mathbf{M}_{\mathrm{MSBL}} = [\boldsymbol{\mu}_{\mathrm{MSBL}_1}, \dots, \boldsymbol{\mu}_{\mathrm{MSBL}_T}] \in \mathbb{C}^{D \times T}$ and the $d$-th row of $\mathbf{M}_{\mathrm{MSBL}}$ is shown as $[\mathbf{M}_{\mathrm{MSBL}}]_{(d,:)}$ [14].

The pseudocode of the MSBL algorithm shown in Figure 3. The MSBL algorithm requires the variance of the noise, $N_0$, to be supplied as an input. The first step of the MSBL is the initialization of the variance parameter vector

$$\hat{\boldsymbol{\gamma}}_{\mathrm{MSBL}} = [\hat{\gamma}_1, \dots, \hat{\gamma}_D] = [1, \dots, 1] = \mathbf{1}_D \tag{18}$$

where $\mathbf{1}_D$ is a column vector of size $D \times 1$ with all its elements equal to 1. Then the MSBL iterates between the E- and M-steps, lines 6-9 (Figure 3), until convergence is achieved, or a fixed number of loops have been run. There is no need to explicitly invert the matrix, $\mathbf{\Omega}_{\mathrm{MSBL}}$, in steps 7 and 8. Instead the Moore-Penrose pseudo-inverse which is way more efficient than explicit matrix inversion can be calculated. The computational complexity of the MSBL algorithm is $O(DM(M+T))$ [16].

1. **begin**
2. **input:** $\boldsymbol{\Phi} = \mathbf{WA}$, $\tilde{\mathbf{Y}}$, $N_0$
3. **initialize:** $\hat{\boldsymbol{\gamma}}_{\mathrm{MSBL}} = [1, \ldots, 1] = \mathbf{1}$
4. **for** $i = 1$: maxIter do
5. $\quad \boldsymbol{\Gamma}_{\mathrm{MSBL}} = \mathrm{diag}\{\hat{\boldsymbol{\gamma}}_{\mathrm{MSBL}}\}$
6. $\quad \boldsymbol{\Omega}_{\mathrm{MSBL}} = N_0\mathbf{I} + \boldsymbol{\Phi}\boldsymbol{\Gamma}_{\mathrm{MSBL}}\boldsymbol{\Phi}^*$
7. $\quad \boldsymbol{\Sigma}_{\mathrm{MSBL}} = \boldsymbol{\Gamma}_{\mathrm{MSBL}} - \boldsymbol{\Gamma}_{\mathrm{MSBL}}\boldsymbol{\Phi}^*\boldsymbol{\Omega}_{\mathrm{MSBL}}^{-1}\boldsymbol{\Phi}\boldsymbol{\Gamma}_{\mathrm{MSBL}}$
8. $\quad \mathbf{M}_{\mathrm{MSBL}} = \boldsymbol{\Gamma}_{\mathrm{MSBL}}\boldsymbol{\Phi}^*\boldsymbol{\Omega}_{\mathrm{MSBL}}^{-1}\tilde{\mathbf{Y}}$
9. $\quad \hat{\gamma}_d = (1/T)\left\|[\mathbf{M}_{\mathrm{MSBL}}]_{(d,:)}\right\|_2^2 + [\boldsymbol{\Sigma}_{\mathrm{MSBL}}]_{(d,d)}, \forall d$
10. **end for**
11. **output:** $\hat{\mathbf{G}}_{\mathrm{MSBL}} = \mathbf{M}_{\mathrm{MSBL}}$, $\hat{\mathbf{H}}_{\mathrm{MSBL}} = \mathbf{A}\hat{\mathbf{G}}_{\mathrm{MSBL}}$, $\hat{\boldsymbol{\gamma}}_{\mathrm{MSBL}}$

**Figure 3.** The pseudocode of the MSBL algorithm

## 3.3. CSBL algorithm

The CSBL algorithm uses a nondiagonal prior covariance matrix to model the correlations between the entries of the path gain vector. The posterior conditional probability density function of $\mathbf{g}_t$ given $\tilde{\mathbf{y}}_t$ is circularly symmetric complex Gaussian with $\mathbf{g}_t \sim \mathcal{CN}(\boldsymbol{\mu}_{\mathrm{CSBL}_t}, \boldsymbol{\Sigma}_{\mathrm{CSBL}}^{-1})$ where the mean vector, $\boldsymbol{\mu}_{\mathrm{CSBL}_t}$, and the posterior precision matrix, $\boldsymbol{\Sigma}_{\mathrm{CSBL}}$, are given [16-17]

$$\boldsymbol{\mu}_{\mathrm{CSBL}_t} = (1/N_0)\boldsymbol{\Sigma}_{\mathrm{CSBL}}^{-1}\boldsymbol{\Phi}^*\tilde{\mathbf{y}}_t \tag{19}$$

$$\boldsymbol{\Sigma}_{\mathrm{CSBL}} = (1/N_0)(\boldsymbol{\Phi}^*\boldsymbol{\Phi}) + \boldsymbol{\Omega}_{\mathrm{CSBL}} \tag{20}$$

respectively. The precision matrix, $\boldsymbol{\Omega}_{\mathrm{CSBL}}$, in Equation (20) is given as

$$\boldsymbol{\Omega}_{\mathrm{CSBL}} = \mathrm{diag}\{\mathbf{c}\}\mathbf{U}^{-1}\mathrm{diag}\{\mathbf{c}\} \tag{21}$$

where $i$-th entry of the parameter vector $\mathbf{c} \in \mathbb{C}^{D\times 1}$ is $c_i = 1/\sqrt{\hat{\gamma}_i}$ and $\mathbf{U}^{-1}$ is the inverse of the correlation coefficient matrix, $\mathbf{U}$ [16-17]. The M-step of the EM algorithm calculates the new parameter vector, $\mathbf{c}_{\mathrm{new}}$, using the old parameter vector, $\mathbf{c}_{\mathrm{old}}$, as in

$$\mathbf{c}_{\mathrm{new}} = \left[\Re\{\mathbf{U}^{-1} \odot \hat{\mathbf{R}}_{\mathbf{g}}^{\mathrm{T}}\}\right]^{-1}\mathbf{c}_{\mathrm{old}} \tag{22}$$

where $\odot$ is the elementwise Hadamard product between two matrices of same dimensions and $\Re\{\cdot\}$ takes the real part of its argument. The estimate of the covariance matrix of the path gain vector in Equation (22) is [16-17]

$$\hat{\mathbf{R}}_{\mathbf{g}} = \boldsymbol{\Sigma}_{\mathrm{CSBL}}^{-1} + \frac{1}{T}\sum_{t=1}^{T}\boldsymbol{\mu}_{\mathrm{CSBL}_t}\boldsymbol{\mu}_{\mathrm{CSBL}_t}^* \tag{23}$$

The pseudocode of the CSBL algorithm is given in Figure 4. The CSBL algorithm requires the coefficient matrix, $\mathbf{U}$, in addition to the noise variance when compared to the pseudocode of the MSBL algorithm in Figure 3. As it can be observed from the pseudocode of the CSBL algorithm (Figure 4), there are two explicit matrix inversion operations in step 8, i.e. the inversion of the post precision matrix $\boldsymbol{\Sigma}_{\mathrm{CSBL}}^{-1}$, and in step 9, i.e. the inversion of the coefficient matrix $\mathbf{U}^{-1}$. Instead of inverting the whole coefficient matrix which is of size $D \times D$, only the submatrix of size $L \times L$ residing within the rows and columns of $\mathbf{U}$ corresponding to the indices of the nonzero entries of $\mathbf{c}$ should be inverted since the rest of nondiagonal elements of the matrix is zero [17]. The computational complexity of the CSBL algorithm is $O(DM(M+T) + D^3)$ [16].

**begin**
**input:** $\boldsymbol{\Phi} = \mathbf{WA}$, $\tilde{\mathbf{Y}}$, $\mathbf{U}$, $N_0$
**initialize:** $\mathbf{c}_0 = [1, \dots, 1] = \mathbf{1}_D$
**for** $i = 1{:}\,\text{maxIter}$ do
    $\boldsymbol{\Omega}_{\text{CSBL}} = \text{diag}\{\mathbf{c}_i\}\mathbf{U}^{-1}\text{diag}\{\mathbf{c}_i\}$
    $\boldsymbol{\Sigma}_{\text{CSBL}} = (1/N_0)(\boldsymbol{\Phi}^*\boldsymbol{\Phi}) + \boldsymbol{\Omega}_{\text{CSBL}}$
    $\mathbf{M}_{\text{CSBL}} = [\boldsymbol{\mu}_{\text{CSBL}_1}, \dots, \boldsymbol{\mu}_{\text{CSBL}_T}] = (1/N_0)\boldsymbol{\Sigma}_{\text{CSBL}}^{-1}\boldsymbol{\Phi}^*\tilde{\mathbf{Y}}$
    $\hat{\mathbf{R}}_{\mathbf{g}} = \boldsymbol{\Sigma}_{\text{CSBL}}^{-1} - (1/T)(\mathbf{M}_{\text{CSBL}}\mathbf{M}_{\text{CSBL}}^*)$
    $\mathbf{c}_i = \left[\Re\{\mathbf{U}^{-1} \odot \hat{\mathbf{R}}_{\mathbf{g}}^{\text{T}}\}\right]^{-1}\mathbf{c}_{i-1}^{-1}$
**end for**
**output:** $\hat{\mathbf{G}}_{\text{CSBL}} = \mathbf{M}_{\text{CSBL}}$, $\hat{\mathbf{H}}_{\text{CSBL}} = \mathbf{A}\hat{\mathbf{G}}_{\text{CSBL}}$, $\hat{\boldsymbol{\gamma}}_{\text{CSBL}} = \mathbf{c}_i^{-1}$

**Figure 4.** The pseudocode of the CSBL algorithm

## 4. Numerical Results

We now compare the normalized mean squared error (NMSE) results of the algorithms. The NMSE obtained via one of the algorithms is calculated as

$$\text{NMSE}_o = 10\log_{10}\left(\frac{1}{R}\sum_{r=1}^{R}\frac{\left\|\hat{\mathbf{H}}_{o,r} - \mathbf{H}_r\right\|_F^2}{\|\mathbf{H}_r\|_F^2}\right) \tag{24}$$

where the total number of Monte Carlo iterations is fixed as $R = 1000$ for each numerical result. $\hat{\mathbf{H}}_{o,r}$ in Equation (24) denotes the estimate of the channel matrix at the $r$-th Monte Carlo iteration, $\mathbf{H}_r = [\mathbf{h}_1 \dots \mathbf{h}_T] \in \mathbb{C}^{N\times T}$, provided by the algorithms, $o \in \{\text{SOMP,MSBL,CSBL}\}$. The NMSE results are shown versus the pilot-to-noise-ratio (PNR) which is defined as

$$\text{PNR} = 10\log_{10}(1/N_0). \tag{25}$$

For all the presented numerical results, the NMSE curves from Equation (24) is plotted against the PNR (Equation (25)) range between 0 dB to 20 dB. For the dictionary matrix, $\boldsymbol{\Phi}$, to be an equal-norm equiangular tight frame, the analog combining matrix is generated according to [9]

$$\mathbf{W} = \mathbf{W}_{\text{BB}}\mathbf{W}_{\text{RF}} = (\mathbf{W}_{\text{RF}}\mathbf{W}_{\text{RF}}^*)^{-1/2}\mathbf{W}_{\text{RF}} \tag{26}$$

where $(\mathbf{W}_{\text{RF}}\mathbf{W}_{\text{RF}}^*)^{1/2}$ is the principal square root of the matrix $\mathbf{W}_{\text{RF}}\mathbf{W}_{\text{RF}}^*$ and each element of $\mathbf{W}_{\text{RF}}$ has a constant amplitude, $1/\sqrt{N}$, and a random phase independent and identically uniformly distributed in $[0,2\pi]$ [9,16]. The conventional least squares (LS) and minimum mean-squared-error (MMSE) estimators are used as benchmark against the algorithms. The LS and MMSE estimators are given as

$$\hat{\mathbf{H}}_{\text{LS}} = (\boldsymbol{\Phi}_{\mathcal{S}}^*\boldsymbol{\Phi}_{\mathcal{S}})^{-1}\boldsymbol{\Phi}_{\mathcal{S}}^*\tilde{\mathbf{Y}} \tag{27}$$

$$\hat{\mathbf{H}}_{\text{MMSE}} = \mathbf{R}_{\mathbf{g}}\boldsymbol{\Phi}_{\mathcal{S}}^*\left(\boldsymbol{\Phi}_{\mathcal{S}}\mathbf{R}_{\mathbf{g}}\boldsymbol{\Phi}_{\mathcal{S}}^* + \frac{1}{N_0}\mathbf{I}_M\right)^{-1}\tilde{\mathbf{Y}} \tag{28}$$

where $\boldsymbol{\Phi}_{\mathcal{S}} = \mathbf{WA}_{\mathcal{S}}$ and $\mathbf{A}_{\mathcal{S}}$ is the submatrix constructed by extracting the columns from $\mathbf{A}$ corresponding to the support of the path gain vector, $\mathcal{S}$. Since these estimators require the support of the path gain vector, $\mathcal{S}$, to be known prior, they are called oracle LS and oracle MMSE respectively. For all the numerical results, the numbers of antennas at the BS and snapshots are fixed at $N = 64$ and $T = 10$ respectively. The column size of the dictionary matrix is set to $D = 128$ and the support of the path gain vector, $\mathcal{S}$, randomly sampled from $\{1, \dots, D\}$ at each Monte Carlo iteration. The entries of the correlation coefficient matrix, $\mathbf{U}$, is generated according to $\rho_{j,k} = \rho^{|j-k|}$ where $\rho = 0.95$.

The NMSE curves plotted in Figure 5 are obtained when the number of nonzero entries of the channel path gain vector is fixed at $L = 4$ and the number of RF chains at the BS is taking values from $M \in \{32,48\}$. The effect of $M$ on the estimation performance is critical since hybrid precoding requires $M < N$ to be power efficient. For both $M$ values, the lowest NMSE results are obtained via the two benchmark methods: the LS and the MMSE estimators. Also due to the small $L$, the performances of the MMSE and the LS are almost equal for high PNR of 20 dB. There is about 2 dB gap between the MMSE for $M = 32$ and the MMSE for $M = 48$. This means that decreasing $M$ from 48 to 32 incur 2 dB penalty on the best attainable estimation performance. Decreasing the number of RF chains result in extra additional noise on the measurements which causes all the NMSE results to increase. The overall best performing algorithm is the CSBL algorithm, while the MSBL algorithm takes the second place. For $M = 48$, the NMSE of the SOMP is the closest to the benchmark methods up to 10 dB. The SOMP results become saturated as the PNR increases beyond 10 dB. This advantage of the SOMP algorithm disappears when the number of RF chains is decreased to $M = 32$. The SOMP algorithm is more sensitive to $M$ compared to the rest of the algorithms.

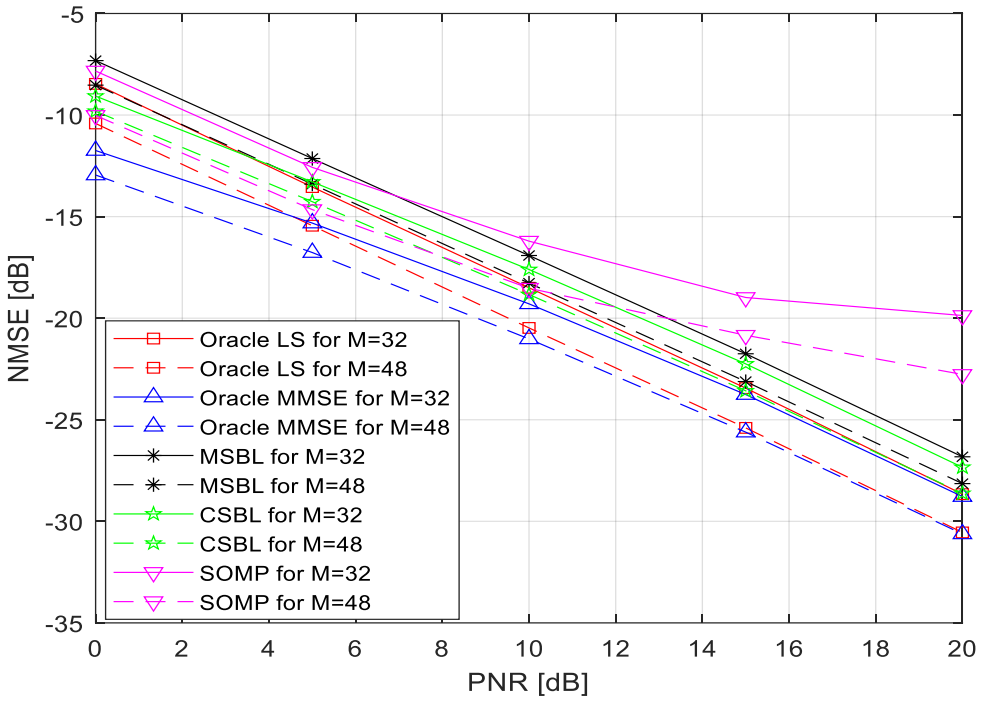


**Figure 5.** NMSE versus PNR for $N = 64$, $T = 10$, $M \in \{32,48\}$ and $L = 4$

Figure 6 shows the NMSE results when the number of RF chains is fixed at $M = 48$ and the number of nonzero taps of the channel path gain vector is taking values from $L \in \{4,16\}$. When $L$ is increased from 4 to 16, the NMSE results of all the algorithms degrades. Also, the correlations between the nonzero entries of the channel vector become more critical on the estimation performance. Since the CSBL algorithm exploits the correlations of the channel vector, its performance remains close to the MMSE estimator. The MSBL algorithm can perform as good as the oracle LS estimator and unlike the oracle LS estimator, the MSBL algorithm does not need the prior knowledge of the path gain vector support. Since the channel is less sparse due to the increased sparsity ratio, the greedy SOMP algorithm gives the highest NMSE curve. For $L = 16$, the CSBL algorithm can follow the lowest NMSE curve obtained via the oracle MMSE estimator with a less than 2 dB PNR gap. The MSBL algorithm is as good as the oracle LS estimator and even better for the PNR range less than 5 dB.

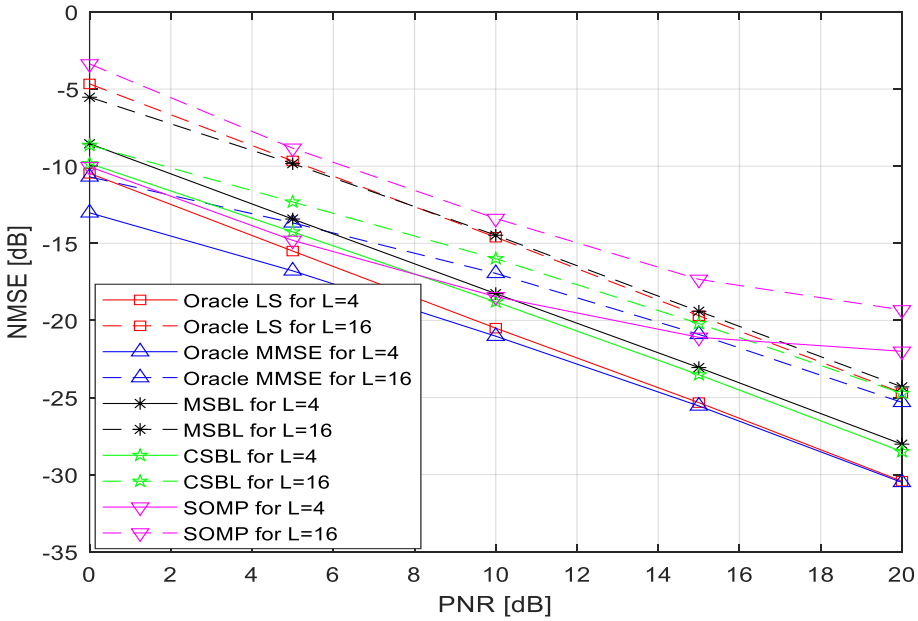


**Figure 6.** NMSE versus PNR for $N = 64$, $T = 10$, $M = 48$ and $L \in \{4,16\}$

The convergence of the NMSE results versus the number of iterations is shown in Figure 7. The number of the mm Wave channel taps and the PNR are fixed at $L = 4$ and 15 dB respectively. The number of the RF chains is $M \in \{32.48\}$ and the number of iterations is varying as $\mathrm{maxIter} \in [10.100]$. The SOMP algorithm always run for fixed number of iterations which is the number of the mmWave channel taps and so its NMSE performance remains constant across varying iterations. The performances of the EM based MSBL and CSBL algorithms depend on the number of iterations. For $M = 32$ at 10 iterations, the gap between the CSBL and the MSBL is almost 10 dB. As the number of iterations increase, the gap diminishes to less than 1 dB. The CSBL algorithm can converge at 60th iteration, while the MSBL algorithm requires 100 iterations for both $M$ values. The CSBL algorithm converges faster and to a lower NMSE level than the MSBL algorithm.

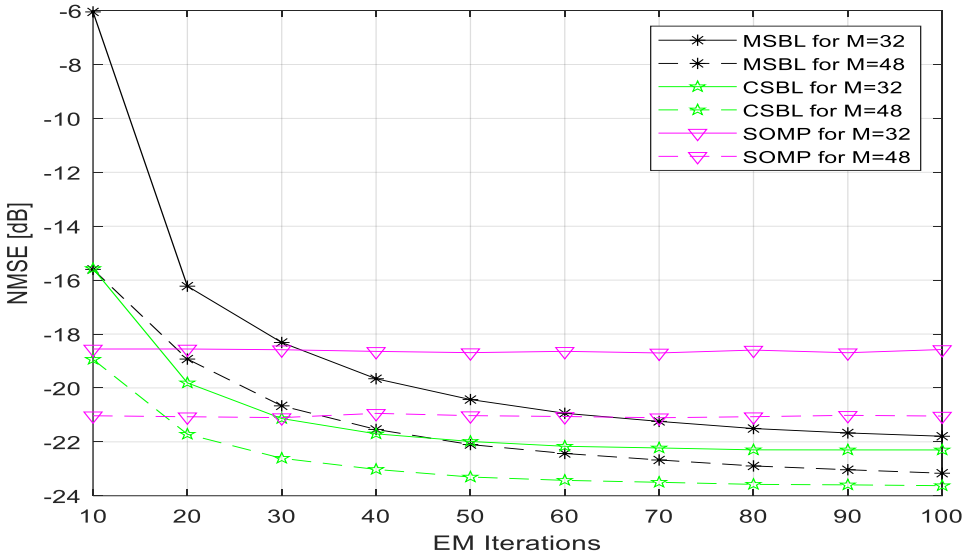


**Figure 7.** NMSE versus number of iterations for $N = 64$, $T = 10$, $M \in \{32,48\}$ and $L = 4$

## 5. Conclusion

This paper investigates sparse signal recovery based covariance estimation of the uplink channel of a single MS in a MIMO mmWave communication system. The BS has a hybrid RF chain and applies the same combining matrix for multiple coherence blocks of the channel estimation phase. We present how the sparse signal recovery algorithms including the SOMP, the MSBL, and the CSBL algorithms can be applied to estimate the covariance of the mmWave channel using the shared combining matrix scheme. The performances of the algorithms are compared in terms of their NMSE against the benchmark oracle MMSE and LS estimators under multiple scenarios with varying number of RF chains and sparsity levels for the mmWave channel. The numerical results show that the performance of the CSBL is superior to the MSBL and the SOMP algorithms for all the considered scenarios. Although the CSBL has superior performance, its computational complexity is the highest due to explicit matrix inversions. The CSBL can exploit the correlations between the nonzero entries of the mmWave channel vector, but the coefficient matrix must be supplied as an input. The coefficient matrix holding the correlations of the mmWave channel vector must be learned before the CSBL can be applied. The MSBL algorithm can be implemented without matrix inversions and so its complexity is much lower compared to the CSBL. However, the MSBL cannot estimate as well as the CSBL and requires the noise variance as an input. The SOMP algorithm, on the other hand, requires the least input and has the lowest computational complexity. Decreasing the number of the RF chains or increasing the number of nonzero entries of the mmWave channel is detrimental to its performance.

## 6. Author Contribution Statement

In the study, Author 1 contributed to conceptualization, data curation, formal analysis, investigation, methodology, validation, visualization, writing – original draft, writing - review and editing.

## 7. Ethics Committee Approval and Conflict of Interest

Ethics committee approval is not needed for preparing the article. There is no conflict of interest for this article.

## 8. References

[1] R. W. Heath, N. González-Prelcic, S. Rangan, W. Roh, and A. M. Sayeed, "An Overview of Signal Processing Techniques for Millimeter Wave MIMO Systems," IEEE J. Sel. Topics Signal Process., vol. 10, no. 3, pp. 436-453, 2016.

[2] T. S. Rappaport, Y. Xing, O. Kanhere, S. Ju, A. Madanayake, and S. Mandal, "Wireless Communications and Applications Above 100 GHz: Opportunities and Challenges for 6G and Beyond," IEEE Access, vol. 7, pp. 78729-78757, 2019.

[3] J. Mo, P. Schniter, and R. W. Heath, "Channel Estimation in Broadband Millimeter Wave MIMO Systems with Few-Bit ADCs," IEEE Trans. Signal Process., vol. 66, no. 5, pp. 1141-1154, 2018.

[4] S. Huang, D. Qiu, and T. D. Tran, "Bayesian Massive MIMO Channel Estimation with Parameter Estimation Using Low-Resolution ADCs," in IEEE ICASSP, Toronto, Canada, pp. 4830-4834, 2021.

[5] R. Zhang, L. Yang, M. Tang, W. Tan, and J. Zhao, "Channel Estimation for mmWave Massive MIMO Systems with Mixed-ADC Architecture," IEEE Open J. Comm. Soc., vol. 4, pp. 606-613, 2023.

[6] X. Yu, J. -C. Shen, J. Zhang, and K. B. Letaief, "Alternating Minimization Algorithms for Hybrid Precoding in Millimeter Wave MIMO Systems," IEEE J. Sel. Topics Signal Process., vol. 10, no. 3, pp. 485-500, 2016.

[7] X. Xue, Y. Wang, L. Yang, J. Shi, and Z. Li, "Energy-Efficient Hybrid Precoding for Massive MIMO mmWave Systems With a Fully-Adaptive-Connected Structure," IEEE Trans. Comm., vol. 68, no. 6, pp. 3521-3535, 2020.

[8] J. Lee, G. -T. Gil, and Y. H. Lee, "Channel Estimation via Orthogonal Matching Pursuit for Hybrid MIMO Systems in Millimeter Wave Communications," IEEE Trans. Comm., vol. 64, no. 6, pp. 2370-2386, 2016.

[9] S. Park, and R. W. Heath, "Spatial Channel Covariance Estimation for the Hybrid MIMO Architecture: A Compressive Sensing-Based Approach," IEEE Trans. Wireless Comm., vol. 17, no. 12, pp. 8047-8062, 2018.

[10] L. Weiland, C. Stöckle, M. Würth, T. Weinberger, and W. Utschick, "OMP with Grid-Less Refinement Steps for Compressive mmWave MIMO Channel Estimation," in IEEE 10th SAM, pp. 543-547, 2018.

[11] C. K. Anjinappa, A. C. Gürbüz, Y. Yapıcı, and İ. Güvenç, "Off-Grid Aware Channel and Covariance Estimation in mmWave Networks," IEEE Trans. Comm., vol. 68, no. 6, pp. 3908-3921, 2020.

[12] R. V. Şenyuva, and E. Anarım, "Multigrid Based Sparse Recovery Method for Multidimensional Harmonic Retrieval," in IEEE 28th SIU, pp. 1-4, 2020.

[13] A. Ali, N. González-Prelcic, and R. W. Heath, "Spatial Covariance Estimation for Millimeter Wave Hybrid Systems Using Out-of-Band Information," IEEE Trans. Wireless Comm., vol. 18, no. 12, pp. 5471-5485, 2019.

[14] D. P. Wipf, and B. D. Rao, "An Empirical Bayesian Strategy for Solving the Simultaneous Sparse Approximation Problem," IEEE Trans. Signal Process., vol. 55, no. 7, pp. 3704-3716, 2007.

[15] Z. Zhang, and B. D. Rao, "Sparse Signal Recovery with Temporally Correlated Source Vectors Using Sparse Bayesian Learning," IEEE J. Sel. Topics Signal Process., vol. 5, no. 5, pp. 912-926, 2011.

[16] D. Prasanna, and C. R. Murthy, "mmWave Channel Estimation via Compressive Covariance Estimation: Role of Sparsity and Intra-Vector Correlation," IEEE Trans. Signal Process., vol. 69, pp. 2356-2370, 2021.

[17] J. N. Pisharody, A. Rajoriya, N. Gupta, and R. Budhiraja, "Fast Correlated SBL Algorithm for Estimating Correlated Sparse Millimeter Wave Channels," IEEE Comm. Letters, vol. 27, no. 5, pp. 1407-1411, 2023.

[18] V. B. Shukla, R. Mitra, O. Krejcar, V. Bhatia, and K. Choi, "Performance Analysis of Sparse Channel Estimators for Millimeter Wave Hybrid MIMO Systems With Non-Ideal Hardware," IEEE Trans. on Veh. Tech., vol. 72, no. 9, pp. 11913-11923, 2023.

[19] T. L. Marzetta, E. G. Larsson, H. Yang, and H. Q. Ngo, Fundamentals of Massive MIMO, Cambridge: Cambridge University Press, 2016.

[20] J. A. Tropp, A. C. Gilbert, and M. J. Strauss, "Algorithms for simultaneous sparse approximation. Part I: Greedy pursuit," EURASIP J. Signal Process., vol. 86, pp. 572-588, 2006.
[21] B. L. Sturm, and M. G. Christensen, "Comparison of orthogonal matching pursuit implementations," in 20th EUSIPCO, pp. 220-224, 2012.